

This is a pre print version of the following article:

Carrier Multiplication in Silicon Nanocrystals:

Theoretical Methodologies and Role of the Passivation / Marri, I.; Govoni, M.; Ossicini, S.. - In: PHYSICA STATUS SOLIDI. C, CURRENT TOPICS IN SOLID STATE PHYSICS. - ISSN 1862-6351. - 14:12(2017), pp. 1700198-1700198. [10.1002/pssc.201700198]

*Terms of use:*

The terms and conditions for the reuse of this version of the manuscript are specified in the publishing policy. For all terms of use and more information see the publisher's website.

18/12/2025 18:59

# Carrier Multiplication in Silicon Nanocrystals: Theoretical Methodologies and Role of the Passivation

Ivan Marri<sup>\*,1</sup>, Marco Govoni<sup>2</sup>, Stefano Ossicini<sup>1,3</sup>

<sup>1</sup> Centro S3, CNR-Istituto Nanoscienze, via Campi 213/a Modena, 41125, Italy

<sup>2</sup> Institute for Molecular Engineering, the University of Chicago, 5747 South Ellis Avenue Chicago, 60637, Illinois (USA)

<sup>3</sup> University of Modena and Reggio Emilia, Department of Science and Methods for Engineering (DISMI) and Centro Interdipartimentale "En&Tech", via Amendola 2 Reggio Emilia, 42122, Italy

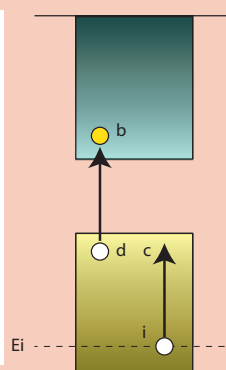
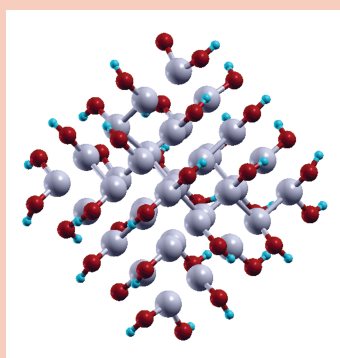
Received XXXX, revised XXXX, accepted XXXX

Published online XXXX

**Key words:** Theoretical Methodologies, Silicon Nanocrystals, Carrier Multiplication.

\* Corresponding author: e-mail marri@unimore.it, Phone: +39 205 5067, Fax: +39 059 2055651

Carrier Multiplication is a non-radiative recombination mechanism that leads to the generation of two or more electron-hole pairs upon absorption of a single photon. By reducing the occurrence of dissipative effects, this process can be exploited to increase solar cell performance. In this work we introduce two different theoretical fully ab-initio methods that can be adopted to study carrier multiplication in nanocrystals. The tools are described in detail and compared. Subsequently we calculate carrier multiplication lifetimes in H- and OH- terminated silicon nanocrystals, pointed out the role played by the passivation on the carrier multiplication processes.



The  $\text{Si}_{35}(\text{OH})_{36}$  nanocrystal is depicted in the left part of the figure. On the right we schematize a Carrier Multiplication decay process started by a hole.

Copyright line will be provided by the publisher

**1 Introduction** The advent of nanoscience and nanotechnologies has opened new perspectives in the development of novel, low dimensional, materials. Control and manipulation of matter on an atomic scale can be exploited to generate novel nanostructured systems where new properties and functionalities are promoted to overcome the limits of traditional semiconductor and organic systems for applications in different fields, from medical devices to drugs and biomedicine, from photonics to energy conversion and thermoelectrics [1–18]. At the nanoscale, elec-

tronic, optical and transport properties can be tuned by size reduction, by changing passivation and shape of the nanostructures, by doping or by surface functionalization. In particular, effects induced by the size reduction can be exploited to promote new recombination processes that are negligible in bulk-like systems. This is the case of the non-radiative Coulomb-driven Carrier Multiplication (CM), that is the counterpart of the Auger recombination [19]. This effect leads to the generation of multiple electron-hole (e-h) pairs after absorption of a single high

Copyright line will be provided by the publisher

energy photon, with an energy at least twice the energy gap of the system. By reducing the occurrence of high-energy dissipative processes and by increasing the number of carriers generated after photon absorption, CM is expected to increase solar cell efficiency. CM has been recorded in a large variety of nanocrystals (NCs) like for instance PbSe and PbS [20–25], CdSe and CdTe [26,27], PbTe [28], InAs [29], Si [30] and Ge [31]. Recently a relevant photocurrent enhancement arising from CM was proven in a PbSe based quantum dot solar-cell [32]. Effects induced on CM dynamics by energy transfer quantum cutting processes were observed [33–35] in Si-NCs organized in a dense array, despite the presence of the observed effect is still under discussion [36]. On a theoretical side, CM has been often described as an impact ionization (II) process that follows the primary photoexcitation event. The II approach was combined with a semi-empirical tight binding model [40–43] to calculate CM rates in PbSe-, PbS- and Si-NCs and with a semiempirical pseudopotential method to estimate biexciton generation rates in CdSe- and InAs-NCs [44]. Similar calculations were also performed within a semi-empirical nonlocal pseudopotential approach [45,46] or using an atomistic pseudopotential method [47,48] to obtain CM rates in CdSe- and PbSe-NCs. Recently a new full ab-initio approach was adopted by M. Govoni et al. [49] and by I. Marri et al. [50–52] to calculate CM lifetimes in systems of isolated and strongly interacting Si-NCs. More complicated models as for instance the coherent superpositions of single- and multi-exciton states and the generation of multi-excitations via virtual single-excitations have been proposed [37–39].

In this work we present new fully ab-initio calculations of CM lifetimes for both spherical hydrogenated and oxygenated Si-NCs. We discuss results obtained using two different theoretical approaches and we investigate, for the first time, CM dynamics in OH-terminated Si-NCs.

**2 Method** In this section we describe the methodologies adopted to calculate CM lifetimes. Following Refs. [40,42,44], CM decay is described as an II process that occurs after the absorption of a single high-energy photon ( $h\nu > 2E_g$ , where  $E_g$  is the energy gap of the system). In this scheme, the decay of a high energy exciton into a biexciton is modeled as the sum of two processes: an electron  $\rightarrow$  negative trion relaxation process (the hole is a spectator, see Fig. 1, decay scheme on the left), and a hole  $\rightarrow$  positive trion relaxation process (the electron is a spectator, see Fig. 1, decay scheme on the right). In this work, electronic structures are calculated from first-principles using the Density Functional Theory (DFT). In particular, Kohn-Sham (KS) states are obtained by solving the KS equation:

$$\hat{H}_{KS}^{k\sigma} \psi_{nk\sigma} = \epsilon_{nk\sigma} \psi_{nk\sigma} \quad (1)$$

where the hamiltonian  $\hat{H}_{KS}^{k\sigma}$  is given by the sum of four terms, the kinetic energy operator and the ionic, Hartree and exchange-correlation potentials. The CM rate

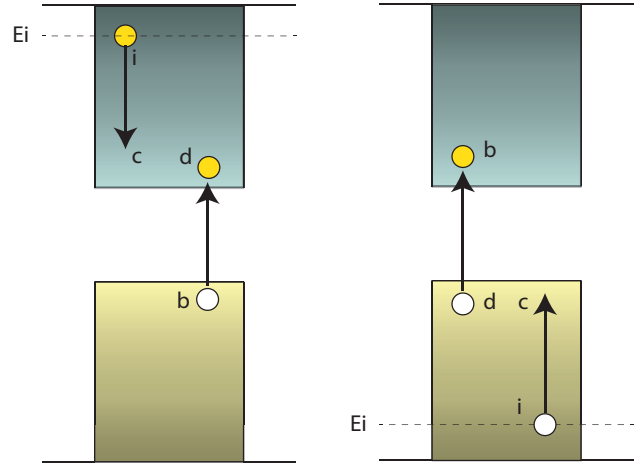


**Figure 1** CM processes ignited by electron (left) and hole (right) relaxation are depicted in the figure.

$R_{n_i, k_i}^e(E_i)$  for mechanisms started by an electron are given by:

$$R_{n_i, k_i}^e(E_i) = \sum_{n_c, n_d}^{cond.} \sum_{n_b}^{val.} \sum_{\mathbf{k}_b, \mathbf{k}_c, \mathbf{k}_d}^{1BZ} 4\pi \left[ |M_D|^2 + |M_E|^2 + |M_D - M_E|^2 \right] \delta(E_i + E_b - E_c - E_d). \quad (2)$$

Similarly, for mechanisms started by a hole, we have:

$$R_{n_i, k_i}^h(E_i) = \sum_{n_c, n_d}^{val.} \sum_{n_b}^{cond.} \sum_{\mathbf{k}_b, \mathbf{k}_c, \mathbf{k}_d}^{1BZ} 4\pi \left[ |M_D|^2 + |M_E|^2 + |M_D - M_E|^2 \right] \delta(E_i + E_b - E_c - E_d) \quad (3)$$

where the indexes  $n$  and  $k$  identify the band and the crystal momentum of the KS state,  $E_i$  is the energy of the carrier that gives rise to the CM mechanism, 1BZ is the first Brillouin zone and  $M_D$  and  $M_E$  are the direct and exchange screened Coulomb matrix elements, respectively. In our simulations, the delta function for energy conservation was implemented in the form of a Gaussian distribution with a full width at half maximum of 0.02 eV. In reciprocal space,  $M_D$  and  $M_E$  assume the form:

$$M_D = \frac{1}{V} \sum_{\mathbf{G}, \mathbf{G}'} \rho_{n_d, n_b}(\mathbf{k}_d, \mathbf{q}, \mathbf{G}) W_{\mathbf{G}\mathbf{G}'} \rho_{n_i, n_c}^*(\mathbf{k}_i, \mathbf{q}, \mathbf{G}')$$

$$M_E = \frac{1}{V} \sum_{\mathbf{G}, \mathbf{G}'} \rho_{n_c, n_b}(\mathbf{k}_c, \mathbf{q}, \mathbf{G}) W_{\mathbf{G}\mathbf{G}'} \rho_{n_i, n_d}^*(\mathbf{k}_i, \mathbf{q}, \mathbf{G}')$$

where both  $\mathbf{k}_c + \mathbf{k}_d - \mathbf{k}_i - \mathbf{k}_b$  and  $\mathbf{G}, \mathbf{G}'$  are vectors of the reciprocal space,  $\mathbf{q} = (\mathbf{k}_c - \mathbf{k}_i)_{1BZ}$  and  $\rho_{n,m}(\mathbf{k}, \mathbf{q}, \mathbf{G}) = \langle \mathbf{n}, \mathbf{k} | e^{i(\mathbf{q} + \mathbf{G}) \cdot \mathbf{r}} | \mathbf{m}, \mathbf{k} - \mathbf{q} \rangle$  is the oscillator strength. The Fourier transform of the screened interaction  $W_{\mathbf{G}, \mathbf{G}'}(\mathbf{q}, \omega)$ , identified by a matrix in  $\mathbf{G}$  and

$\mathbf{G}'$  is evaluated at  $\omega = 0$  and assumes the form;

$$W_{\mathbf{G},\mathbf{G}'}(\mathbf{q}, 0) = v_{\mathbf{G},\mathbf{G}'}^{\text{bare}}(\mathbf{q}) + W_{\mathbf{G},\mathbf{G}'}^p(\mathbf{q}, 0) = \frac{4\pi \cdot \delta_{\mathbf{G},\mathbf{G}'}}{|\mathbf{q} + \mathbf{G}|^2} + \frac{\sqrt{4\pi e^2}}{|\mathbf{q} + \mathbf{G}|} \bar{\chi}_{\mathbf{G},\mathbf{G}'}(\mathbf{q}, 0) \frac{\sqrt{4\pi e^2}}{|\mathbf{q} + \mathbf{G}'|}. \quad (4)$$

The first term ( $v_{\mathbf{G},\mathbf{G}'}^{\text{bare}}(\mathbf{q})$ ) of Eq. (4) denotes the bare Coulomb interaction while the second one ( $W_{\mathbf{G},\mathbf{G}'}^p(\mathbf{q}, 0)$ ) includes the screening caused by the medium. In Eq. (4),  $\bar{\chi}_{\mathbf{G},\mathbf{G}'}(\mathbf{q}, 0)$  is the symmetrized reducible polarizability. Noticeably,  $W_{\mathbf{G},\mathbf{G}'}^p(\mathbf{q}, 0)$  is often given as a function of the reducible polarization  $\chi_{\mathbf{G},\mathbf{G}'}(\mathbf{q}, 0)$ , where:

$$\bar{\chi}_{\mathbf{G},\mathbf{G}'}(\mathbf{q}, 0) = \frac{\sqrt{4\pi e^2}}{|\mathbf{q} + \mathbf{G}|} \chi_{\mathbf{G},\mathbf{G}'}(\mathbf{q}, 0) \frac{\sqrt{4\pi e^2}}{|\mathbf{q} + \mathbf{G}'|}. \quad (5)$$

Obviously Eqs. 4 and 5 hold also when  $\omega \neq 0$ . The reducible polarizability is connected to the irreducible polarizability  $\chi_{\mathbf{G},\mathbf{G}'}^0$  by the Dyson equation that, in the Random Phase Approximation (RPA), assumes the form:

$$\chi_{\mathbf{G},\mathbf{G}'} = \chi_{\mathbf{G},\mathbf{G}'}^0 + \sum_{\mathbf{G}_1, \mathbf{G}_2} \chi_{\mathbf{G},\mathbf{G}_1}^0 v_{\mathbf{G}_1, \mathbf{G}_2}^{\text{bare}} \chi_{\mathbf{G}_2, \mathbf{G}'}.$$

The presence of off-diagonal elements in the solution of the Dyson equation is related to the inclusion of the local fields (LFs) that stem from the breakdown of the translational invariance imposed by the lattice.

Different strategies have been adopted to calculate Eq. (4), and in particular the term  $W_{\mathbf{G},\mathbf{G}'}^p(\mathbf{q}, \omega)$ . Two of them will be here discussed and then applied to calculate CM lifetimes in Si-NCs.

The first one permits to develop the noninteracting response function  $\chi_{\mathbf{G},\mathbf{G}'}^0$  in terms of the non-interacting (bare) Green's function, that is:

$$\begin{aligned} \chi_{\mathbf{G},\mathbf{G}'}^0(\mathbf{q}, \omega) = & 2 \sum_{n,n'} \int_{BZ} \frac{d\mathbf{k}}{(2\pi)^3} \rho_{n',n}^*(\mathbf{k}, \mathbf{q}, \mathbf{G}) \rho_{n',n}(\mathbf{k}, \mathbf{q}, \mathbf{G}') \times \\ & \left[ \frac{f_{n\mathbf{k}-\mathbf{q}}(1-f_{n'\mathbf{k}})}{\omega + \epsilon_{n,\mathbf{k}-\mathbf{q}} - \epsilon_{n',\mathbf{k}} + i0^+} - \frac{f_{n\mathbf{k}-\mathbf{q}}(1-f_{n'\mathbf{k}})}{\omega + \epsilon_{n',\mathbf{k}} - \epsilon_{n,\mathbf{k}-\mathbf{q}} - i0^+} \right] \end{aligned} \quad (6)$$

where  $f_{n\mathbf{k}}$  is the occupation factor of the  $|n\mathbf{k}\rangle$  state. Eq. (6) is note as Adler-Wiser [53,54] expression of the irreducible polarizability. This method will be refereed as the non-interacting Green's function (NIGF) procedure in the following. We applied this methodology in the works of Refs. [49,50], where a modified version of the code Yambo [55] was used to calculate CM rates in systems of isolated and interacting Si-NCs. Relation (6) implies a sum over both occupied and unoccupied states. Due to the complexity of the procedure, that leads to the calculation of a large number of matrix elements (this number depends on the

size of the system, on the number of electrons, on the kinetic energy cutoff used for the wavefunctions etc.), the NIGF often requires a truncation of the reducible density-density response function  $\chi_{\mathbf{G},\mathbf{G}'}$ . In Refs. [49], for instance, we imposed energy cutoffs ranging from 0.5 to 1.5 Hartree and we obtained, for the largest systems,  $\chi_{\mathbf{G},\mathbf{G}'}$  matrices with a size of about  $22500 \times 22500$ .

The second one, defined projective eigendecomposition of the dielectric screening (PDEP) [56–60], implies a spectral decomposition of the symmetrized irreducible polarizability, that occurs through an iterative projection of the eigenvectors of  $\bar{\chi}_{\mathbf{G},\mathbf{G}'}^0(\mathbf{q}, 0)$  via repeated linear-response computations within the density functional perturbation theory (DFPT) and iterative diagonalization algorithm [61,62]. In this approach the symmetrized irreducible polarizability is developed as:

$$\bar{\chi}_{\mathbf{G},\mathbf{G}'}^0(\mathbf{q}, 0) = \sum_{i,j}^{N_{pdep}} \phi_i(\mathbf{q} + \mathbf{G}) \lambda_{i,j} \phi_j^*(\mathbf{q} + \mathbf{G}') \quad (7)$$

where the  $N_{pdep}$   $\phi_i$  vectors are iteratively calculated by solving the Sternheimer equation [63] without explicitly evaluating empty states. Initially a set of orthogonal  $N_{pdep}$  basis functions with random components is defined. Then a given perturbation  $V_i^{\text{pert}} = \phi_i$  is applied and the linear variation  $\Delta\psi_{nk\sigma}$  of the occupied eigenstates  $\psi_{nk\sigma}$  is calculated using the relation:

$$(H_{KS}^{\sigma} - \epsilon_{nk\sigma}) \hat{P}_c^{\mathbf{k}\sigma} \Delta\psi_{nk\sigma}(r)^i = -\hat{P}_c^{\mathbf{k}\sigma} V_i^{\text{pert}} \psi_{nk\sigma}(r)^i \quad (8)$$

where  $\hat{P}_c^{\mathbf{k}\sigma}$  is the projector operator over the occupied manifold of states with momentum  $\mathbf{k}$  and spin  $\sigma$ . Finally Eq. (8) is solved iteratively by using, for instance, the preconditioned conjugate-gradient method. The linear variation of the density induced by the  $i$ -th perturbation is then obtained by:

$$\Delta n_i(r) = \sum_{\sigma} \sum_{n=1}^{N_{occ}^{\sigma}} \int_{BZ} \frac{d\mathbf{k}}{(2\pi)^3} [\psi_{nk\sigma}(r)^* \Delta\psi_{nk\sigma}^i(r) + cc] \quad (9)$$

and the matrix elements of the irreducible polarizability in the space spanned by  $\phi_i$  are calculated using the relation  $\bar{\chi}_{ij}^0 = \langle \phi_i | \Delta n_j(r) \rangle$ . The matrix is then diagonalized to obtain a new set of basis vectors  $\phi_i$  and the procedure is iterated using a Davidson algorithm as implemented in the WEST code [58].

After the calculation of both direct and exchange Coulomb matrix elements using both the NIGF and PDEP procedures, CM rates are obtained (Eq. (2) and (3)). CM lifetimes are then calculated as reciprocal of rates and are given as a function of the energy of the initial carrier  $E_i$ .

**3 Results** Two different types of Si-NCs with a different passivation are analyzed in this work: hydrogenated

and oxygenated Si-NCs. These systems are obtained by terminating the surface dangling bonds with H- and with OH- (hydroxyls functional group), respectively. This section is divided in two parts. Initially we apply and compare the methods described in Section 2 to calculate CM lifetimes for a simple H-terminated Si-NC. Subsequently we extend our analysis to consider an oxygen passivated Si-NC; CM lifetimes are then calculated using the PDEP procedure. To our knowledge, it is the first time that a fully ab-initio calculation is performed to evaluate effects induced by different surface passivations on the CM activity. The systems here considered are the  $\text{Si}_{35}\text{H}_{36}$ -NC, already analyzed in the works of Ref. [49], and the  $\text{Si}_{35}(\text{OH})_{36}$ -NC. As pointed out in Ref. [18], this configuration describe adequately a system formed by a Si-NC encapsulated in a  $\text{SiO}_2$  matrix. The electronic structure is calculated using the density functional theory plane-wave pseudopotential PWscf code of the Quantum-ESPRESSO package [64]; silicon, hydrogen and oxygen norm-conserving pseudopotentials are adopted and the local density approximation LDA is used to calculate the exchange-correlation functional. For the fully hydrogenated system we adopt a kinetic energy cutoff for wavefunctions of 35 (55) Ry for the H- (OH-) terminated Si-NCs. A simple cubic cell with a lattice parameter of 90 a.u. is adopted for the H-terminated system (this values is reduced to 70 a.u. when the PDEP procedure is adopted, in order to reduce the number of G vectors and therefore the computational cost of the simulation). A cubic FCC cell with a lattice parameters of 95 a.u. is employed for the OH-terminated Si-NC. In our approach, multiexciton configurations are calculated without including many-body corrections.

**3.1 H-terminated Si-NCs: a direct comparison between two different tools** In this section we report the calculated CM lifetimes for the  $\text{Si}_{35}\text{H}_{36}$ -NC. In particular, we compare the results obtained with the two procedures of section 2, that is the so called NIGF method of Eq. (6) and the PDEP procedure, Eq (7) [65]. The methodology of Eq. (6) has been applied by imposing an energy cutoff of 1.5 Hartree to the screening term. A spectral decomposition on 1300 basis vectors is instead adopted in the PDEP methodology.

Calculated CM lifetimes for mechanisms ignited by hole relaxation are reported in the Fig. 2. Here different colors indicated the different methodology used in the simulation. Crosses and dots, instead, identify the lifetimes calculated considering only the bare term of Eq. (4) or both the bare and the screened term of Eq. (4). Following the conclusions of Ref. [49] we do not consider contributions due to the vacuum states. As a consequence for the  $\text{Si}_{35}\text{H}_{36}$ -NC electron-initiated CM mechanisms are energetically forbidden. In Fig. 2, the zero of the energy scale is placed at half gap. CM lifetimes calculated using the NIGF procedure extend for about 2 eV above the CM energy threshold (we consider the same window of energies of Ref [49]). The calculations performed with the PDEP method, in-

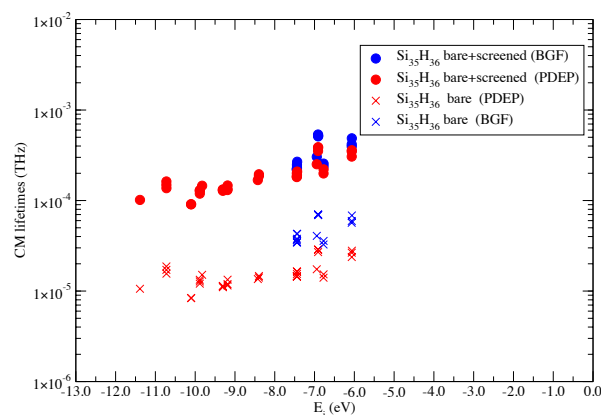


**Figure 2** CM lifetimes for the  $\text{Si}_{35}\text{H}_{36}$ -NC are reported. The lifetimes are calculated following two different tools and using different terms (see text).

stead, was extended to  $\sim 6$  eV below the CM energy threshold.

Results of Fig. 2 point out that:

1. CM lifetimes calculated using the NIGF and PDEP approach are very similar,
2. CM is very fast and settle to fraction of femtosecond in the range of energies analyzed,
3. the inclusion of the screened part of the Coulomb interaction is very important: when the second term in Eq. (4) is not considered, CM move to lower lifetimes of about one order of magnitude.

Point one confirms the robustness and reliability of the two procedures adopted in the calculation of CM processes in Si-NCs. Depending on the size and characteristic of the system and on the features of the platform where simulations are performed (number of nodes, number of core per nodes, memory per core, parallel architecture typology, etc..) one method can be more efficient than the other, but if the convergence is correctly achieved (truncation of the reducible density-density  $\chi_{G,G'}$  and number of PDEP basis) the two procedures lead to similar results. The small differences detectable in Fig. 2 (CM lifetimes are slightly lower when the PDEP procedure is adopted, both for the bare and the bare+screened cases) are probably due to the different size of the cell used in the simulations (90 a.u., that is 3.66 times the diameter of the Si-NC, for the calculation performed with the NIGF technique, 70 a.u., that is 2.85 times the diameter of the Si-NC, for the calculation performed with the PDEP procedure) and by the fact that the NIGF method was applied by adopting an exact box-shaped Coulomb cut-off technique in order to remove the spurious Coulomb interaction among replicas (see Ref. [66]).

**3.2 OH-terminated Si-NCs, role played by the surface passivation.** In this section we extend our analysis to the study of CM processes in OH- terminated

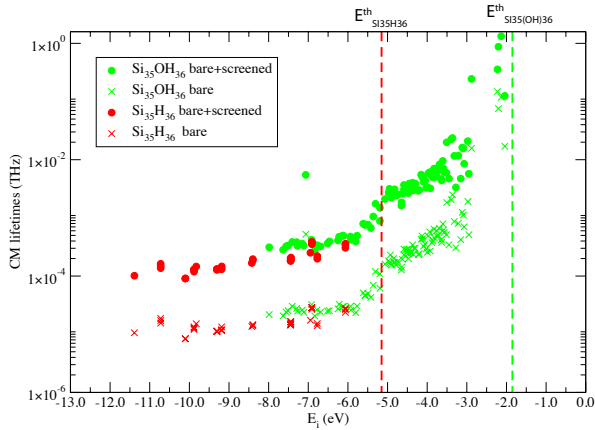


**Figure 3** Hole relaxation CM lifetimes for both the  $\text{Si}_{35}(\text{OH})_{36}$ -NC and the  $\text{Si}_{35}\text{H}_{36}$ -NC are reported on an absolute energy scale. Red and green vertical dashed lines denote the CM energy threshold for the H- and OH- terminated Si-NC, respectively.

Si-NCs. A direct comparison with the results obtained in section 3.1 will permit to shed light on the role played by surface passivation on the CM activity. As pointed out by different authors, H-passivation represents a very simple Si-NCs surface termination that is, in some cases, far from the one observed in realistic samples. For this reason we investigated a more complicated system, that is the  $\text{Si}_{35}(\text{OH})_{36}$ -NC, where the structure is obtained from H-terminated Si-NC by replacing hydrogens with hydroxyls functional groups (OH); the Si-NC is then relaxed. The choice of OH groups as Si-NCs passivation has several reasons: as proven in Ref. [33], beside strain effects, there are important similarities between the calculated electronic and optical properties for silica embedded Si-NCs and the Si-NCs passivated with OH groups. Moreover this passivation allows to take contact with experiments performed on all-inorganic colloidal Si-NCs terminated by OH [67]. Following section 3.1, we considered only relaxation mechanisms started by a hole, although for this system the energy conservation rule allows also mechanisms ignited by electron relaxation. CM lifetimes for the  $\text{Si}_{35}(\text{OH})_{36}$ -NC are obtained using the PDEP procedure, with 2100 vectors basis for the calculation of the symmetrized irreducible polarizability. Calculated CM lifetimes are reported in Fig. 3 (CM lifetimes are here represented using the so called absolute energy scale) and in Fig. 4 (here a relative energy scale is adopted) and compared with the one obtained for the  $\text{Si}_{35}\text{H}_{36}$ -NC.

In Fig. 3 both the pure bare (crosses) and the bare+screened (dots) contributions are reported. Due to the different LDA energy gaps (3.42 eV for the  $\text{Si}_{35}\text{H}_{36}$ -NC and 1.23 eV for the  $\text{Si}_{35}(\text{OH})_{36}$ -NC), Si-NCs show different activation CM energy threshold  $E_{\text{Si}_{35}\text{H}_{36}}^{\text{th}}$  and  $E_{\text{Si}_{35}(\text{OH})_{36}}^{\text{th}}$ , that are identified by the red and the green vertical dashed lines,

respectively (see Fig. 3). Obviously, CM is theoretically permitted at lower energies when the OH passivation is taken into account.

Two important details emerge from the analysis of plots of Fig. 3. First at all, also for the  $\text{Si}_{35}(\text{OH})_{36}$ -NC, a first-principle calculation of the CM lifetimes requires an accurate evaluation of the screened term  $W_{\mathbf{G},\mathbf{G}'}^p(\mathbf{q}, 0)$  in Eq. (4), and in particular a detailed treating of the local fields effects that cannot be evaluated by using oversimplified models. By only including the bare term in the screened interaction, CM lifetimes move to lower values of about one order of magnitude. Secondly, CM lifetimes decrease more rapidly in the  $\text{Si}_{35}\text{H}_{36}$ -NC with respect to the  $\text{Si}_{35}(\text{OH})_{36}$ -NC and settle to femtoseconds just few tenths of eV below  $E_{\text{Si}_{35}\text{H}_{36}}^{\text{th}}$ . Remarkably, at low energies, that is far from the activation threshold  $E_{\text{Si}_{35}(\text{OH})_{36}}^{\text{th}}$ , CM lifetimes seems to be almost independent on the passivation [68]. From  $-6$  eV to  $-8$  eV, for instance, red and green dots (crosses) are almost overlapped (starting from the CM energy threshold, for both the considered Si-NCs, we have calculated CM lifetimes in a window of energies of about 6 eV. Due to the large number of possible CM decay paths, which increases when the range of considered energies  $E_i$  increases, we cannot extend the range of energies considered in the calculations, and for the  $\text{Si}_{35}(\text{OH})_{36}$ -NC, we cannot consider CM transitions for energy  $E_i$  below  $\approx -8$  eV). Noticeably  $E_i$  denotes the energy of the carrier starting the process calculated with respect to the midgap. As a consequence, when Si-NCs of different  $E_g$  are considered,  $E_i$  identifies carriers that are placed at a different distance with respect the band edge. For this motive we introduce a new parameter, called  $E_{i_r}$ , that represents the distance in energy between the carrier starting the CM process and the band edge (in our specific case the valence band edge). For mechanisms ignited by hole relaxation we have:  $E_{i_r} = -(|E_i| - |E_{\text{gap}}/2|)$ . For the systems consid-

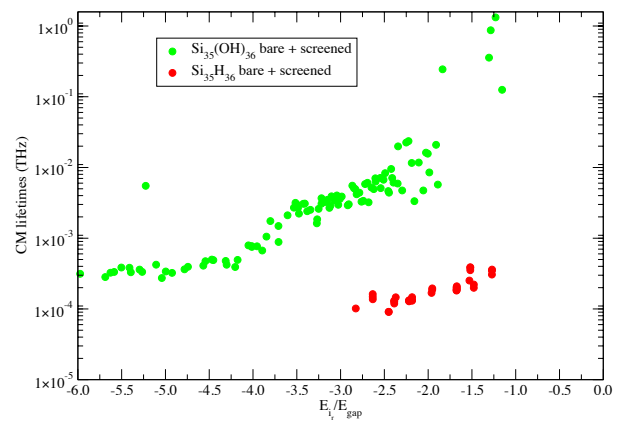


**Figure 4** Hole relaxation CM lifetimes for both the  $\text{Si}_{35}(\text{OH})_{36}$ -NC and the  $\text{Si}_{35}\text{H}_{36}$ -NC are reported adopted a relative energy scale.



ered in this work we have  $\left| E_{i_r}^{Si_{35}H_{36}} \right| < \left| E_{i_r}^{Si_{35}(OH)_{36}} \right|$ . This is consisted with Ref. [40], where it is stated that CM rates are proportional to the product of an effective screened Coulomb matrix element and of the density of final states at the energy  $E_i$  ( $\rho_f(E_i)$ ).  $\rho_f(E_i)$  depends on the electronic properties of the system and increases with  $E_{i_r}$ . In general,  $\rho_f(E_i)$  is larger in the OH-terminated system than in the H-terminated one, that is:  $\rho_f(E_i)_{Si_{35}(OH)_{36}} > \rho_f(E_i)_{Si_{35}H_{36}}$ . At the same time, far from the activation threshold, for a fixed value of  $E_i$ , H-terminated Si-NCs shows higher effective screened Coulomb matrix elements as a consequence of the strong confinement of the charge density induced by the hydrogens. Far from the activation threshold therefore, we have a sort of compensation between these two effects (Coulomb interaction higher in the H-terminated system with respect to the OH-terminated one and  $\rho_f(E_i)$  higher in the OH-terminated systems with respect to the H-terminated one) that leads, at a fixed values of  $E_i$ , to similar CM lifetimes for the  $Si_{35}(OH)_{36}$ -NC and the  $Si_{35}H_{36}$ -NC.

Results of panel (a) are not sufficient to understand the effects induced by CM on the population of the excited states. To be effective, CM has to dominate over all the other recombination and relaxation mechanisms, and in particular the hot carrier cooling via phonon emission. In Fig. 4, we report the calculated CM lifetimes as a function of the ratio  $E_{i_r}/E_{gap}$ , that is by adopting the so called relative energy scale (here the sign minus indicates that processes are induced by hole relaxation). As pointed out by M. C. Beard et al. Ref. [69], this plot provides more information about the competition between CM with other energy relaxation channels. When this scale is adopted, we observe that CM is more efficient in  $Si_{35}H_{36}$ -NC than in  $Si_{35}(OH)_{36}$ -NC. The presence of oxygen at the surface, therefore, can reduce the relevance of the CM processes, making thus more complicated the possibility of observing multiple excitons generations upon absorption of a single high-energy photon.

**4 Conclusions** In this work we have calculated CM lifetimes in Si-NCs. Our calculations have been performed using two different (largely diffused) methodologies, which enable the calculation of the screened Coulomb interaction by using the non-interacting electron-hole Green's function method and the projective eigendecomposition of the dielectric screening procedure. For the considered systems, the two methodologies lead to very similar results. Both of them point out the importance of a detailed description of the screening caused by the medium and of the local fields terms, that are fundamental when the screened Coulomb interaction is calculated. We have then compared CM lifetimes of H-terminated and OH-terminated Si-NCs. We have proven that the presence of oxygen at the surface reduces the theoretical CM activation threshold. When an absolute energy scale is adopted, far from the activation threshold, CM lifetimes seems to

be independent on the passivation. In order to have a more general comprehension of the effect, we have also analyzed CM decay paths adopting a relative energy scale, that permits to have more information about the competition between CM with other energy relaxation channels. When a relative energy scale is adopted we observe that CM processes are more efficient in H-terminated than in OH-terminated Si-NCs. This work represents a first, important, step toward the comprehension of the mechanisms that connect CM decay processes with Si-NCs passivation and open new perspective for future analysis on larger and more complicated NCs. An analysis of this type is fundamental to improve the comprehension of the microscopic mechanisms that rule CM in low-dimensional systems and can complement experimental activities in the engineering of new third-generation nanostructured solar cell devices.

**5 Acknowledgement** The authors thank the Super-Computing Interuniversity Consortium CINECA for support and high-performance computing resources under the Italian Super-Computing Resource Allocation (ISCRA) initiative, PRACE for awarding us access to resource FERMI IBM BGQ, and MARCONI HPC cluster based in Italy at CINECA. Stefano Ossicini thank the Centro Interdipartimentale "En&Tech" that supported his research activity. Ivan Marri thank the Centre of Excellence MaX – MAterials at the eXascale – (grant no. 676598) that supported his research activity.

## References

- [1] F. Erogbobo, K. T. Yong, I. Roy, G. X. Xu, P. N. Prasad, and M. T. Swihart, *ACS Nano* **2**, 873–878 (2008).
- [2] B. F. P. McVey, S. Prabakar, J. J. Goodig, and R. D. Tilley, *ChemPlusChem* **82**, 60–73 (2017).
- [3] N. Daldosso and L. Pavesi, *Laser & Photon. Rev.* **3**, 508–534 (2009).
- [4] D. V. Talapin, J. S. Lee, M. V. Kovalenko, and E. V. Shevchenko, *Chem. Rev.* **110**, 389–458 (2010).
- [5] I. Marri and S. Ossicini, *Solid State Comm.* **147**, 205 – 207 (2008).
- [6] R. Guerra, I. Marri, R. Magri, L. Martin-Samos, O. Pulci, E. Degoli, and S. Ossicini, *Superlattices and Microstructures* **46**, 246 – 252 (2009).
- [7] M. A. Green, *Prog. Photovolt: Res. Appl.* **9**, 123–135 (2001).
- [8] S. Ossicini, O. Bisi, E. Degoli, I. Marri, F. Iori, E. Luppi, R. Magri, R. Poli, G. Cantele, D. Ninno, F. Trani, M. Marsili, O. Pulci, V. Olevano, M. Gatti, K. Gaal-Nagy, A. Incze, and G. Onida, *J. Nanosci. Nanotechnol.* **8**, 479–492 (2008).
- [9] A. J. Nozik, *Nano Lett.* **10**, 2735 (2010).
- [10] E. Degoli, R. Guerra, F. Iori, R. Magri, I. Marri, O. Pulci, O. Bisi, and S. Ossicini, *C. R. Physique* **10**, 575 – 586 (2009).
- [11] M. S. Dresselhaus, C. Gang, Y. T. Ming, Y. Ronggui, L. Hohyun, W. Dezhi, R. Zhifeng, J. P. Fleurial, and P. G. Adv. Mater. **19**, 1043–1053 (2007).

- [12] T. Claudio, N. Stein, D. G. Stroppa, B. Klobes, M. M. Koz, P. Kudejova, N. Petermann, H. Wiggers, G. Schierning, and R. P. Hermann, *Phys. Chem. Chem. Phys.* **16**, 25701–25709 (2014).
- [13] F. Iori, E. Degoli, E. Luppi, R. Magri, I. Marri, G. Cantele, D. Ninno, F. Trani, and S. Ossicini, *J. Lum.* **121**, 335–339 (2006).
- [14] A. Iacomino, G. Cantele, D. Ninno, I. Marri, and S. Ossicini, *Phys. Rev. B* **78**, 075405 (2008).
- [15] F. Priolo, F. Gregorkiewicz, M. Galli, and T. F. Krauss, *Nature Nanotechnol.* **1**, 19–32 (2014).
- [16] F. Iori, E. Degoli, R. Magri, I. Marri, G. Cantele, D. Ninno, F. Trani, O. Pulci, and S. Ossicini, *Phys. Rev. B* **76**, 085302 (2007).
- [17] Z. Bisadi, M. Mancinelli, S. Manna, S. Tondini, M. Bernard, A. Samusenko, M. Ghulinyan, G. Fontana, P. Bettotti, F. Ramiro-Manzano, G. Pucker, and L. Pavesi, *Phys. Status Solidi A* **212**, 2659–2671 (2015).
- [18] R. Guerra, I. Marri, R. Magri, L. Martin-Samos, O. Pulci, E. Degoli, and S. Ossicini, *Phys. Rev. B* **79**(Aug), 155320 (2009).
- [19] M. Govoni, I. Marri, and S. Ossicini, *Phys. Rev. B* **84**, 075215 (2011).
- [20] R. J. Ellingson, M. C. Beard, J. C. Johnson, P. Yu, O. I. Micic, A. J. Nozik, A. Shabaev, and A. L. Efros, *Nano Lett.* **5**, 865–871 (2005).
- [21] R. D. Schaller and V. I. Klimov, *Phys. Rev. Lett.* **92**, 186601 (2004).
- [22] M. T. Trinh, A. J. Houtepen, J. M. Schins, T. Hanrath, J. Piris, W. Knulst, A. P. L. M. Goossens, and L. D. A. Siebbeles, *Nano Lett.* **8**, 1713–1718 (2008).
- [23] G. Nair, S. M. Geyer, L. Y. Chang, and M. G. Bawendi, *Phys. Rev. B* **78**, 125325 (2008).
- [24] R. D. Schaller, M. Sykora, J. M. Pietryga, and V. I. Klimov, *Nano Lett.* **6**, 424–429 (2006).
- [25] R. D. Schaller, M. A. Petruska, and V. I. Klimov, *Appl. Phys. Lett.* **87**, 253102 (2005).
- [26] R. D. Schaller, M. Sykora, S. Jeong, and V. I. Klimov, *J. Phys. Chem. B* **110**, 25332–25338 (2006).
- [27] D. Gachet, A. Avidan, I. Pinkas, and D. Oron, *Nano Lett.* **10**, 164–170 (2010).
- [28] J. E. Murphy, M. C. Beard, A. G. Norman, S. P. Ahrenkiel, J. C. Johnson, P. Yu, O. I. Micic, R. J. Ellingson, and A. J. Nozik, *J. Am. Chem. Soc.* **128**, 3241–3247 (2006).
- [29] R. D. Schaller, J. M. Pietryga, and V. I. Klimov, *Nano Lett.* **7**, 3469–3476 (2007).
- [30] M. C. Beard, K. P. Knutsen, P. Yu, J. M. Luther, Q. Song, W. K. Metzger, R. J. Ellingson, and A. J. Nozik, *Nano Lett.* **7**, 2506–2512 (2007).
- [31] S. Saeed, P. Stallinga, F. C. Spoor, A. J. Houtepen, L. D. Siebbeles, and T. Gregorkiewicz, *Light: Science and Applications* **4** (2015).
- [32] O. E. Semonin, J. M. Luther, S. Choi, H. Y. Chen, J. Gao, A. J. Nozik, and M. C. Beard, *Science* **334**, 1530–1533 (2011).
- [33] D. Timmerman, I. Izeddin, P. Stallinga, Y. I. N., and T. Gregorkiewicz, *Nature Photon.* **2**, 105–109 (2008).
- [34] D. Timmerman, J. Valenta, K. Dohnalova, W. D. A. M. de Boer, and T. Gregorkiewicz, *Nature Nano.* **6**, 710–713 (2011).
- [35] M. T. Trinh, R. Limpens, W. D. A. M. de Boer, J. M. Schins, L. D. A. Siebbeles, and T. Gregorkiewicz, *Nature Photon.* **6**, 316–321 (2012).
- [36] J. Valenta, M. Greben, S. Gutsch, D. Hiller, and M. Zacharias, *Appl. Phys. Lett.* **105**, 243107 (2014).
- [37] A. Shabaev, A. L. Efros, and A. J. Nozik, *Nano Lett.* **6**, 2856–2863 (2006).
- [38] R. D. Schaller, V. M. Agranovich, and V. I. Klimov, *Nature Phys.* **1**, 189–194 (2005).
- [39] E. Rabani and R. Baer, *Chem. Phys. Lett.* **496**, 227–235 (2010).
- [40] G. Allan and C. Delerue, *Phys. Rev. B* **73**, 205423 (2006).
- [41] G. Allan and C. Delerue, *Phys. Rev. B* **77**, 125340 (2008).
- [42] G. Allan and C. Delerue, *Phys. Rev. B* **79**, 195324 (2009).
- [43] C. Delerue, G. Allan, J. J. H. Pijpers, and M. Bonn, *Phys. Rev. B* **81**, 125306 (2010).
- [44] E. Rabani and R. Baer, *Nano Lett.* **8**, 4488–4492 (2008).
- [45] M. Califano, A. Zunger, and A. Franceschetti, *Nano Lett.* **4**, 525–531 (2004).
- [46] M. Califano, A. Zunger, and A. Franceschetti, *Appl. Phys. Lett.* **84**, 2409–2411 (2004).
- [47] A. Franceschetti, J. M. An, and A. Zunger, *Nano Lett.* **6**, 2191–2195 (2006).
- [48] A. Franceschetti and Y. Zhang, *Phys. Rev. Lett.* **100**, 136805 (2008).
- [49] M. Govoni, I. Marri, and S. Ossicini, *Nature Photon.* **6**, 672–679 (2012).
- [50] I. Marri, M. Govoni, and S. Ossicini, *J. Am. Chem. Soc.* **136**, 13257–13266 (2014).
- [51] I. Marri, M. Govoni, and S. Ossicini, *Beilstein J. Nanotech.* **6**, 343–352 (2015).
- [52] I. Marri, M. Govoni, and S. Ossicini, *Solar Energy Materials and Solar Cells* **145**, 162–169 (2016).
- [53] S. L. Adler, *Phys. Rev.* **126**(2), 413–420 (1962).
- [54] N. Wiser, *Phys. Rev.* **129**(1), 62–69 (1963).
- [55] A. Marini, C. Hogan, M. Grüning, and D. Varsano, *Comput. Phys. Commun.* **180**, 1392–1403 (2009).
- [56] H. V. Nguyen, T. A. Pham, D. Rocca, and G. Galli, *Phys. Rev. B* **85**, 081101 (2012).
- [57] T. A. Pham, H. V. Nguyen, D. Rocca, and G. Galli, *Phys. Rev. B* **87**, 155148 (2013).
- [58] M. Govoni and G. Galli, *J. Chem. Theory Comput.* **11**, 2680–2696 (2015).
- [59] H. F. Wilson, F. Gygi, and G. Galli, *Phys. Rev. B* **78**, 113303 (2008).
- [60] H. F. Wilson, D. Lu, F. Gygi, and G. Galli, *Phys. Rev. B* **79**, 245106 (2009).
- [61] S. Baroni, P. Giannozzi, and A. Testa, *Phys. Rev. Lett.* **58**, 1861–1864 (1987).
- [62] S. Baroni, S. de Gironcoli, A. Dal Corso, and P. Giannozzi, *Rev. Mod. Phys.* **73**, 515–562 (2001).
- [63] R. M. Sternheimer, *Phys. Rev.* **96**, 951–968 (1954).
- [64] P. Giannozzi, S. Baroni, N. Bonini, M. Calandra, R. Car, C. Cavazzoni, D. Ceresoli, G. L. Chiarotti, M. Cococcioni, I. Dabo, A. D. Corso, S. de Gironcoli, S. Fabris, G. Fratesi, R. Gebauer, U. Gerstmann, C. Gougoussis, A. Kokalj, M. Lazzeri, L. Martin-Samos, N. Marzari, F. Mauri, R. Mazzarello, S. Paolini, A. Pasquarello, L. Paulatto, C. Sbraccia, S. Scandolo, G. Sclauzero, A. P. Seitsonen, A. Smogunov, P. Umari, and R. M. Wentzcovitch, *J. Phys.-Cond. Mat.* **21**, 395502 (2009).



- [65] M. Vörös, D. Rocca, G. Galli, G. T. Zimanyi, and A. Gali, Phys. Rev. B **87**, 155402 (2013).
- [66] C. A. Rozzi, D. Varsano, A. Marini, E. K. U. Gross, and A. Rubio, Phys. Rev. B **73**, 205119 (2006).
- [67] H. Sugimoto, M. Fujii, J. Fukuda, K. Imakita, and K. Akamatsu, Nanoscale **6**, 122–126 (2014).
- [68] Our results point out that CM processes are slightly faster in the H-terminated system. However, at the same energies, the differences between the CM lifetimes calculated for the  $\text{Si}_{35}(\text{OH})_{36}\text{-NC}$  and the  $\text{Si}_{35}\text{H}_{36}\text{-NC}$  are very small; we cannot exclude that these differences raise from the approximations used in the simulations.
- [69] M. C. Beard, A. G. Midgett, M. C. Hanna, J. M. Luther, B. K. Hughes, and A. J. Nozik, Nano Lett. **10**, 3019–3027 (2010).